www.EFCF.com/Lib
ISBN 978-3-905592-23-8

B0304 (Published elsewhere)

Characterization of the local morphology at triple-phase boundaries after SOFC/SOEC operation

G. Rinaldi (1), A. Nakajo (1), M. Cantoni (2), W.K.S. Chiu (3), J. Van herle (1)
(1) Group of Energy Materials, École Polytechnique Fédérale de Lausanne, Switzerland
(2) Interdisciplinary Centre for Electron Microscopy, École Polytechnique Fédérale de Lausanne, Switzerland
(3) Department of Mechanical Engineering, University of Connecticut, Storrs, USA
giorgio.rinaldi@epfl.ch

Abstract

The evolution of a Ni-YSZ microstructure under operation comprises the coarsening and the decrease of the contiguity of the Ni phase. The process occurs faster in the first thousand hours of operation and results in the progressive degradation of electrochemical performance because of the reduced density of connected triple-phase boundaries (TPB). A clear correlation between TPB density and performance of the solid oxide cell has been demonstrated over the past years. However, the effect of operation on the morphology of the Ni and YSZ surfaces near the TPBs is still unclear, despite the expected relevance for the electrode performance. Indeed, the gas species are first adsorbed on the surface of each solid phase and then diffuse to the TPBs before electrochemical reaction.

Different Ni-YSZ cermet samples operated under solid oxide fuel cell (SOFC) and electrolysis (SOEC) conditions were imaged by 3-D focused ion beam - scanning electron microscopy (FIB-SEM) serial sectioning. Properties including phase size distribution, interfacial surface areas, and total and connected TPB density were first measured, before further characterization of the morphology close to the TPBs. A spilling algorithm was developed to characterize the surface available for diffusion on the YSZ and Ni surfaces for each TPB. Because the algorithm proceeds slice by slice, each diffusion surface is first treated as a line and referred to as an “available length”. The measurements along the three scanning directions of an analyzed volume are then merged for quantitative analyses. The evolution upon aging of the Ni available length distributions exhibited a slight diminution of the spread, resulting in a gathering toward a peak value (around 0.3 µm) and in a progressive decrease of the lengths larger than 0.5 µm. In the YSZ case, a shift toward larger lengths was observed, characterized by an increase of the modal value from 0.8 to 1 µm while maintaining a similar skewness. The behaviour during SOEC operation deviated for the two available measurements for the SOFC case.

A percolation model that uses standard 3-D measurements as input was developed to investigate the evolution of the measured available lengths using simple geometrical concepts. The percolation model confirms the expected correlation between the growth of the particles and the decrease of total TPB lengths, likely related to a diminution of the number of particles per unit of volume. A sensitivity analysis was performed to capture the relationship between Ni coarsening and the increase of YSZ available lengths observed in the imaged samples.

The study suggests a complex relationship between network and local morphology properties that are likely relevant for the effective electrocatalytic properties of the TPBs. The understanding of the correlations is expected to help improving both the electrode initial performance and the durability.

ISBN 978-3-905592-23-8

Introduction

A main contribution to the microstructural alterations in the solid oxide cell (SOC) fuel electrode is the agglomeration of Ni due to high mobility and low wettability to the YSZ surface. The evolution of the phase diameter has been extensively studied in the literature in the light of Ostwald ripening to explain the process, since the size of the Ni particles tends to grow at the expense of the smaller ones [1-2]. Analyses have been performed to establish a more detailed understanding encompassing the interaction between the phases, such as Zener pinning [2], and topological coarsening theory, which is based on the evolution of a connected network rather than a dispersion of separate particles [3]. Microstructural evolution is enhanced by the high temperature of SOC operation (750°C corresponds to 62% of the Ni melting point). Moreover, Ni coarsening lowers the effective three-phase boundary (TPB) density as well as the connectivity of the Ni phase, causing a progressive loss of performance [4-5]. A consequent reduction of the contact area with pores and YSZ is also commonly observed.

Since the evolution of the microstructure tends to a lower energy level, material migrates from regions with high curvature (with larger chemical potential) to lower-curvature surfaces, when the mobility is sufficiently large for the time scale of the observation. According to Davis et al. [6], the propensity of the Ni-YSZ microstructure to the agglomeration of particles is in part due to high dihedral angles (~117°), which ultimately leads to a depletion of connected electrochemical sites, mainly due to the loss of percolation. The growth of the Ni phase mainly occurs during the first 500 hours of the SOC lifetime [2-7-8].

Questions however remain on the evolution regime in the long-term, for the prediction of electrode performance degradation over periods corresponding to the current lifetime target of a SOC device. Further, the evolution of the YSZ microstructure has not been sufficiently clarified in full detail. The ceramic phase is often considered close to static, since the diffusion coefficient of Zr^{4+} is seven orders of magnitude lower than that of Ni [6]. The quantification of even a mild evolution is likely relevant, since studies have highlighted interaction between the phases, where the YSZ phase hinders the evolution of Ni particles following a Zener pinning mechanism [2]. Relocation of YSZ during time has been reported in a few cases [1-4-9-10-11], which may allow further Ni rearrangement.

The electrode performance depends not only on the number of connected TPBs and the transport properties of the phases [12], but also likely on the local morphology in the proximity of the active electrochemical regions. A gradient of adsorbed species is likely present on Ni and YSZ surfaces under polarization. The size and morphology of the diffusion surfaces can locally differ in the complex, reticulate and evolving Ni-YSZ microstructure, potentially leading to a limitation of electrochemical performance, whenever the gradient is constrained on a region that is not sufficiently extended. The objective of the present study is therefore to assess the impact of Ni-YSZ microstructure evolution on both the standard and local morphological properties near the TPBs. First, the quantification of volume averaged metric and topological properties of four samples is performed, respectively: one in pristine condition, two after fuel cell operation (SOFC) for 1900 h and 4700 h, and one after electrolysis operation (SOEC) for 10700 h. The analysis is then extended to the measurement of the “available lengths”, which are defined as the regions on which the surface species can diffuse under polarization. Lastly, the measured distributions are discussed in the light of a percolation theory-based model to better understand the effect on the variation of these properties due to Ni coarsening.

ISBN 978-3-905592-23-8

Experiments and Characterization

The imaging and analysis of the accessible TPB properties of the four volumes to be studied here were presented in a previous work [12]. The two SOFC volumes were tested under dry H_2 diluted with N_2. The sample operated for 1,900 h at 750°C belonged to a segmented-cell and exhibited an increase in area specific resistance mainly during the first 50 h. The second sample, operated for 4,700 h at 780°C, was part of a 6-cell short stack characterized by a fairly constant voltage degradation rate of 0.8% kh^{-1}. Lastly, the SOEC sample was tested for 10700 h at 720°C under 90% H_2O and 10% H_2. In this case, the degradation was severe during the initial 2,000 h, with a voltage increase rate of 4% kh^{-1} on average and then stabilized below 0.5% kh^{-1}. The stack survived accidental water interruption incidents and was stopped after the fourth interruption. All the samples were imaged close to the interface with the electrolyte by focused ion beam - scanning electron microscopy (FIB-SEM) serial sectioning.

Parameters including volume fractions, median diameter (d50), total and connected TPB lengths, interfacial surface areas (ISA) and total surface areas measurements were computed from the 3-D reconstructions, based on the methods previously developed [12-14].

A measurement procedure based on a spilling algorithm was developed to characterize the surface available for diffusion on Ni and YSZ near the TPBs. Starting from each TPB, the algorithm spills over the Ni and YSZ interfacial surfaces in contact with the pores following the evolution of the local morphology (proceeding slice by slice). The developed routine also verifies that each voxel belonging to the considered solid phase is in contact with at least one pore voxel to guarantee the consistency along the followed path. The algorithm stops in the case of the detection of a new TPB or an external border of the slice along the path (in the last case, the measurement is not considered by default in the analysis). Isotropy in terms of available length was observed in all the volumes investigated in the present study. The results obtained for each direction are then merged, to obtain a distribution of “available lengths” on Ni and YSZ.

Results and Discussion

The measured topological properties are reported in Table 1 and Figs. 1A-C. The net increase of d50 (35% after 4700 h of operation in SOFC mode) clearly indicates the growth of the Ni phase. The measurements indicate also a slight increase of the median YSZ diameter (9% after 4700 h), which is not negligible and would suggest that the ceramic phase slightly evolves during operation as well. Measurements for longer operation time will be required to confirm this trend. The Ni growth rate appears close to constant over the investigated time range in the SOFC-aged samples, but this is not reflected in a monotonic decrease of the total TPB length (especially after 1900 h). Instead, the density of connected TPB shows a decrease, highlighting the effects of a reduction in connectivity likely because of necking and/or pinch-off. It is also interesting to note that the Ni-YSZ ISA decreases from the beginning, while the Ni-pores ISA at 1900 h is still similar to the initial value. On the other hand, the YSZ-pores ISA does not significantly change over time. The total surface of Ni and YSZ shown in Fig. 1 also monotonically decreases until 4700 h.

ISBN 978-3-905592-23-8

Table 2: Metric and topological properties measured on the pristine and aged Ni-YSZ volumes. The standard deviation is indicated in parenthesis. ISA values were adjusted by multiplying with the factor π/6 to estimate the actual surface area from the digitized volume assuming close to spherical shapes.

		Pristine	SOFC 1900 h	SOFC 4700 h	SOEC 10700 h
Dimensions X-Y-Z [µm]	-	17.1-10.0-18.5	16.6-10.7-16.7	21.0-12.0-19.5	9.7-9.7-9.7
Voxel size [nm]	-	7	7	10	10
Volume fraction	Pore	0.28 (0.01)	0.26 (0.01)	0.30 (0.01)	0.27 (0.01)
	YSZ	0.43 (0.01)	0.45 (0.01)	0.43 (0.01)	0.42 (0.01)
	Ni	0.29 (0.01)	0.29 (0.01)	0.27 (0.01)	0.31 (0.01)
d50 [µm]	YSZ	0.36 (0.01)	0.39 (0.01)	0.40 (0.01)	0.39 (0.01)
	Ni	0.45 (0.01)	0.53 (0.01)	0.61 (0.01)	0.65 (0.01)
Total TPB length [µm/µm^3]	-	9.0 (0.1)	9.1 (0.2)	5.6 (0.1)	6.3 (0.1)
Connected TPB length [µm/µm^3]	-	7.3 (0.1)	6.7 (0.3)	4.5 (0.1)	5.1 (0.2)
Interfacial surface area [µm^2/µm^3]	Pore-YSZ	1.51 (0.05)	1.59 (0.03)	1.59 (0.02)	1.56 (0.03)
	Pore-Ni	0.53 (0.02)	0.54 (0.03)	0.32 (0.01)	0.35 (0.01)
	Ni-YSZ	1.31 (0.05)	1.09 (0.04)	0.97 (0.01)	0.98 (0.02)
Total surface area [µm^2/µm^3]	Pore	2.04 (0.05)	2.13 (0.03)	1.92 (0.02)	1.91 (0.03)
	YSZ	2.83 (0.05)	2.67 (0.04)	2.56 (0.02)	2.54 (0.03)
	Ni	1.84 (0.05)	1.63 (0.04)	1.29 (0.01)	1.33 (0.02)

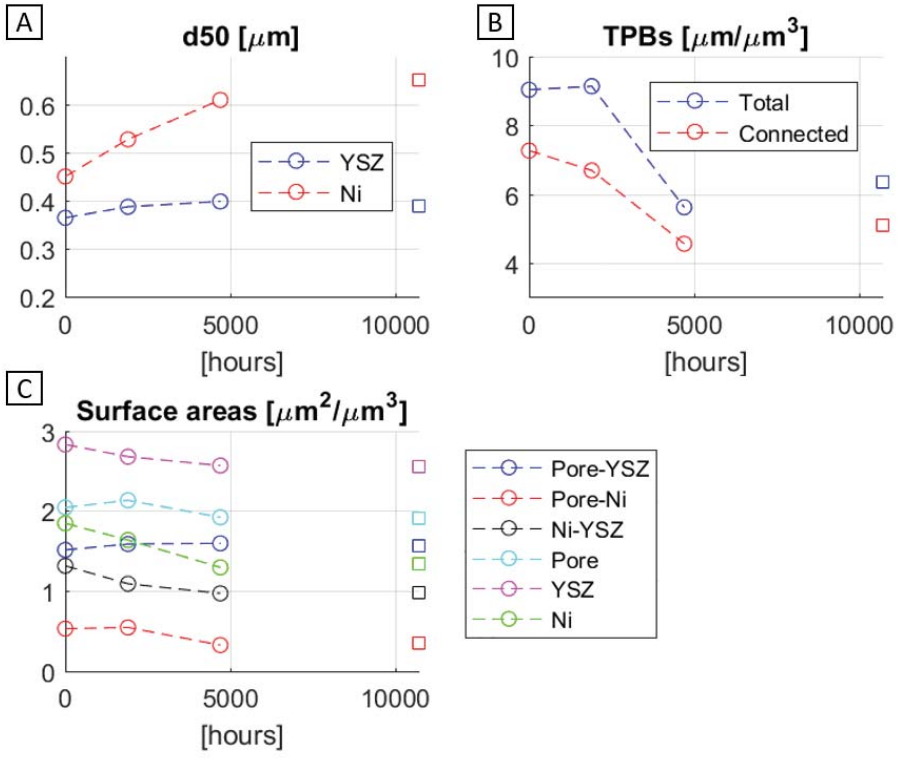

Figure 3: Evolution of measured topological properties (data referred to Table 1). SOFC aged values are displayed with circle, SOEC aged with a square. (A) Ni and YSZ d50. (B) Total and connected TPB lengths. (C) Interfacial and total surface areas.

ISBN 978-3-905592-23-8

The evolution of the SOEC sample differs from the SOFC ones, exhibiting a lower TPB reduction, despite a significantly longer exposure to operation temperature. The total and connected TPBs are larger with respect to the operation in SOFC mode after 4700 h, but the ISA are in contrast similar. Differences were further noticeable within the SOEC sample when comparing the regions up to approximately the first 4 µm next to the electrolyte and further away. The depletion of Ni close to the interface resulted in a finer but less connected Ni microstructure [12]. This therefore indicates a potential variation in the Ni transport mechanism between SOFC and SOEC conditions.

The analysis based on standard measurements presented above has been extended by the measurement of diffusion surfaces, using the concept of "available length" introduced in the section "Experiments and Characterization". The goal is to analyze how the morphology of the surface near the TPB evolves in operation and to infer the potential consequences for electrochemical performance. In a stereological approach, such surfaces are rather considered as lengths associated to a TPB point. An average estimate of the available lengths can be computed as the ratio between the ISA and total TPB length. This calculation is expected to provide a lower estimation of the diffusion length. It indeed assumes that an interfacial surface area unit element is assigned to a single TPB, whereas in the reticulate Ni-YSZ microstructure the surfaces available for diffusion are expected to overlap. The results of such preliminary calculations listed in Table 2 indicate a constant value of Ni lengths after SOFC operation, with a slight diminution in the SOEC case. The ceramic phase instead presents a net increase of such lengths, implying a possible improvement of the apparent charge-transfer resistance that depends on surface diffusive reactions on YSZ.

Table 3: Averaged available lengths on Ni and YSZ.

	Pristine	**SOFC 1900 h**	**SOFC 4700 h**	**SOEC 10700 h**
Averaged Ni available length [µm]	0.059	0.060	0.058	0.055
Average YSZ available length [µm]	0.167	0.174	0.284	0.246

Figs. 2A-B reports the computed Ni and YSZ available lengths. The logarithmic distributions are number-weighted. The trends roughly follow those of Table 2. On the leftward part of the two plots, the dashed lines indicate the portion of distributions lower than four times the voxel size of the reconstructed volumes. The voxel size is 7 nm for pristine and 1900 h, 10 nm for 4700 h and 10700 h. As shown, the plots exhibit scatter for lengths lower than approximately 40 nm. The peak of the YSZ distribution is located at around 1 µm, while in the Ni case, it is around a smaller value of 0.3 µm. A likely reason is the larger pore-YSZ interfacial surface. In general, the evolution upon aging of the distributions exhibit different trends: the spread of the available lengths on Ni slightly decreases, resulting in a gathering toward the peak values, causing a progressive diminution of the lengths larger than 0.5 µm. The results indicate in contrast a shift toward larger lengths with time for the ceramic phase, maintaining a similar skewness, based on visual inspection. This clear difference in trends may inform about the specific morphological evolution for the two phases. Moreover, the behaviour during SOEC operation does not follow the monotonic trends observed in the available SOFC samples.

ISBN 978-3-905592-23-8

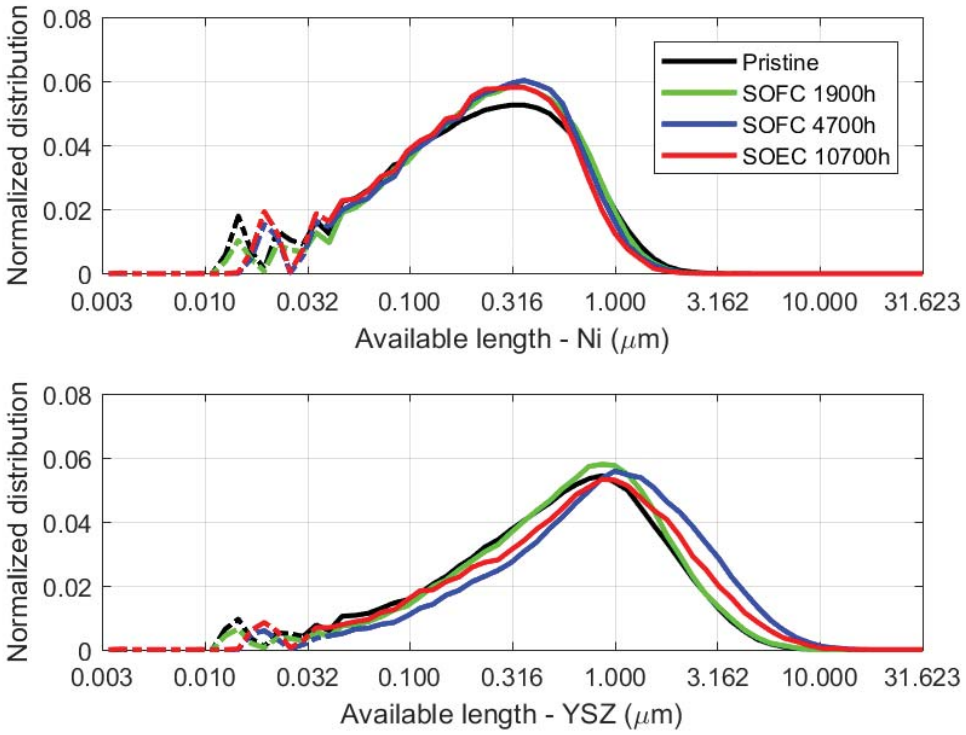

Figure 2: (A), (B) Ni and YSZ available lengths logarithmic distributions.

A percolation theory-based model was developed to investigate the reasons for the measured topological properties and inform about the effects of the coarsening of the Ni phase on the measured available length. The approach consists in combining percolation theory and the topological properties measured on the reconstructions obtained by FIB-SEM serial sectioning (Table 1). The percolation theory relies on the prediction of contact numbers among neighbouring spherical particles (defined as coordination numbers) [15]. The size and the connection of these particles are computed by assigning the measured d50 of Ni and YSZ, volume fractions, and ISAs. In the developed approach, all the particles within a same phase are monosized, but the ratio of radii for Ni and YSZ can be varied. This assumption stems from the percolation model used in the present study [15]. TPB lengths are considered as the intersection circumference between metallic and ceramic particles. Moreover, the contact angles are measured between the centre of the spherical particles and their intersection (also between particles of the same type). Those angles differ from the so-called “dihedral angles”, which are between two intersecting surfaces of different phases and are not considered in the present analysis. Lastly, the Ni available lengths are defined as the shortest path between YSZ particles equally spaced on the surface of the commonly shared Ni particle (and vice-versa for the YSZ available lengths). The computed values of the contact angles, TPB density and available lengths computed using percolation theory are reported in Figs. 3A-C.

ISBN 978-3-905592-23-8

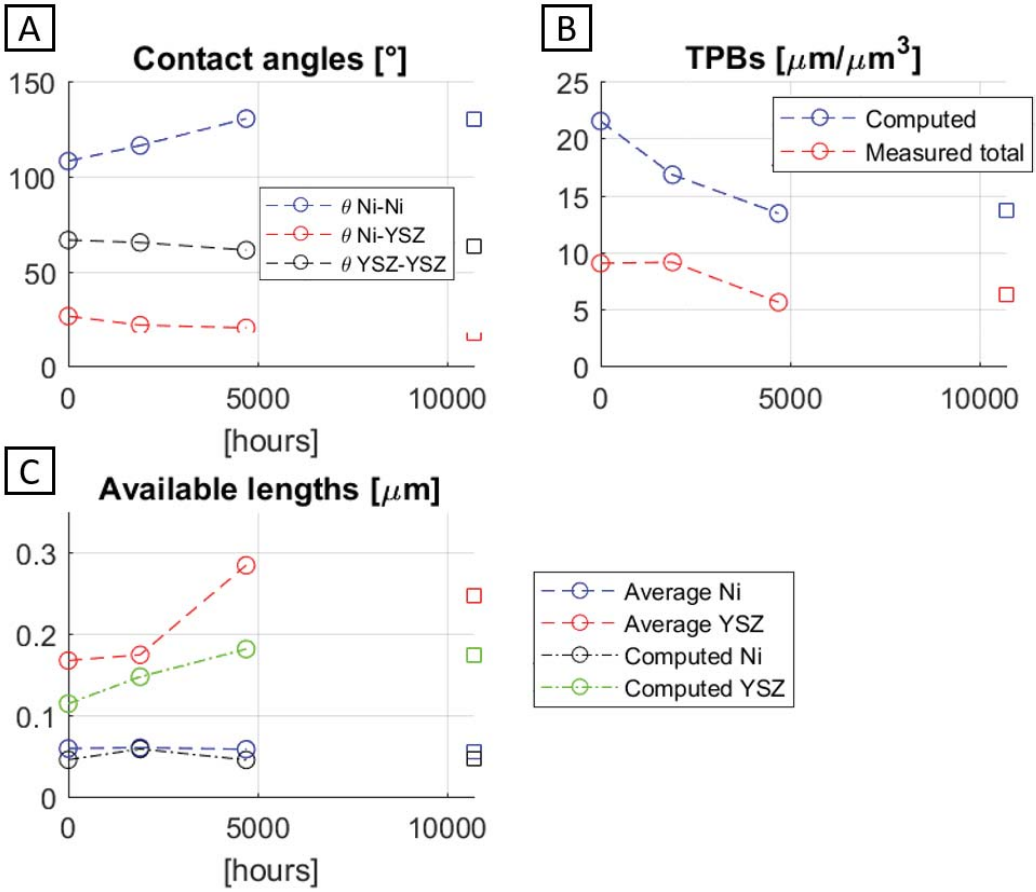

Figure 3: percolation theory-based model results. SOFC aged values are displayed with circle, SOEC aged ones with a square. (A) Contact angles between particles. (B) Total TPB lengths computed and measured (from Table 1). (C) Computed Ni and YSZ available lengths and computed averages (from Table 2).

The trend in the computed available lengths is similar to the average values reported in Table 2, characterised by a slight evolution of Ni lengths and a progressive increase of the ceramic phase until 4700 h. The total TPB density also shows a similar trend, apart from the decrease at 1900 h not observed in the FIB-SEM reconstructions. The contact angle θ Ni-Ni tends to increase over time, corresponding to an overall agglomeration of Ni particles according to the coarsening process. Because of the intrinsic limitation of the approach assuming monosized particles, the model is not amenable for discussing the effects of necking.

A sensitivity analysis with the percolation theory-based model was performed to better understand the effect of Ni coarsening on the available length. The size of the spherical particles and the contact angles were individually increased to highlight the effect on TPBs, available lengths and surface areas. The d50's were augmented up to 50% from the initial values reported in Table 1. The Ni-Ni and Ni-YSZ contact angles were varied over a broader range compared to what is displayed in Fig. 3A. The results are presented qualitatively in Table 3 using arrows to inform about the main effects, which are related to the correlated properties, and then compared with the measured and computed data reported in Figs. 1 and 3.

ISBN 978-3-905592-23-8

Table 4: Qualitative results of the sensitivity analysis (arrow - increase/decrease, dash – no significant change).

		d50 Ni ↗	d50 YSZ ↗	θ Ni-Ni ↗	θ Ni-YSZ ↗
Total TPB	-	↘	↘	-	↗
Available lengths	YSZ	-	↗	-	↘
	Ni	↘	↗	↘	↘

The percolation model confirms the expected correlation between the growth of the particles and the decrease of total TPB lengths, likely related to a diminution of the number of particles per unit of volume. The increase of detected YSZ available lengths over time appears caused by the slight increase of the YSZ d50 and the decrease of contact angle θ Ni-YSZ. Coarsening of the Ni phase instead does not seem to have a direct significant effect. On the other hand, the increase of the Ni d50 and of the Ni-Ni contact angle would have an inverse effect on Ni-related available length. Hence, the progressive decrease of the more extended lengths displayed in Fig. 2A (around 1 μm) may be related to the agglomeration of larger inclusions. Similarly to the YSZ case, this effect is partially balanced by the increase of YSZ d50 and decrease of θ Ni-YSZ, as indicated by the close to constant computed values in Fig. 3C. Moreover, under the assumption that the dihedral angles do not change over time, the contact angles θ Ni-YSZ may vary only in presence of a change in size, thus its change is indirectly related to the particle growth. Lastly, θ YSZ-YSZ values were not reported in Table 3 since they did not clearly show a strong effect on the selected properties.

Conclusions

The evolution of the Ni-YSZ electrode microstructure under operation has been investigated by measuring and analyzing the metric and topological properties obtained from reconstructed 3-D FIB-SEM volumes. The agglomeration of the metallic and ceramic (to an extend that requires additional measurements for confirmation) phases up to 4700 h of SOFC operation was observed to cause a diminution of the total and connected TPB lengths. The concurrent decrease of the Ni and YSZ total surface area without a major change in volume fraction suggests an accretion of larger inclusions at the expense of the smaller ones. SOEC operation resulted in slightly higher values of detected TPB lengths despite the similar mean size and surface areas compared to the SOFC 4700 h aged volume.

The distribution of available diffusion lengths associated to each TPB displayed a reduction of the spread in the Ni case, resulting in a progressive decrease of extended lengths (up to 1 μm) and an accumulation toward the peak values (around 0.3 μm). YSZ length distributions exhibited a net shift toward higher values. The percolation model based on standard 3-D measurements captured the previous trends, and in particular exhibited a net increase of the contact angles between Ni particles, which is directly related to the agglomeration of the larger inclusions. A sensitivity analysis indicated a correlation between the available lengths of both phases and the size distribution of YSZ. Therefore, a slight increase in the YSZ size distribution appears as the main reason for the shift of the YSZ length distribution. The coarsening of the metallic regions would instead cause a diminution of the larger Ni detected lengths.

ISBN 978-3-905592-23-8

Acknowledgements

This work was supported by the Swiss EOS Holding Ph. D. thesis funding (G. Rinaldi), contract 2014-0365. The research also received funding from the Fuel Cells and Hydrogen 2 Joint Undertaking under grant agreement No 735692 (Project name: CH2P) and under grant agreement No 735918 (Project name: INSIGHT). This Joint Undertaking receives support from the European Union's Horizon 2020 research and innovation program, from Hydrogen Europe and Hydrogen Europe Research. Swiss partners in these H2020 projects receive funding from the Swiss Secretariat in Education, Research and Innovation (SEFRI), under contracts 16.0199 (Insight) and 16.0223 (CH2P). WKSC acknowledges financial support from the National Science Foundation (Award CBET-1134052), and an Energy Frontier Research Center on Science Based Nano-Structure Design and Synthesis of Heterogeneous Functional Materials for Energy Systems (HeteroFoaM Center) funded by the US Department of Energy, Office of Science, Office of Basic Energy Sciences (Award DE-SC0001061).

References

[1] L. Holzer, B. Iwanschitz, Th. Hocker, B. Münch, M. Prestat, D. Wiedenmann, U. Vogt, P. Holtappels, J. Sfeir, A. Mai, Th. Graule, Journal of Power Sources 196 (2011), 1279-1294.
[2] G. J. Nelson, K. N. Grew, J. R. Izzo Jr., J. J. Lombardo, W. M. Harris, A. Faes, A. Hessler-Wyser, J. Van herle, S. Wang, Y. S. Chu, A. V. Virkar, W. K.S. Chiu, Acta Materialia 60 (2012), 3491-3500.
[3] R. T. Dehoff, "A General Theory of Microstructural Evolution by Surface Diffusion," Sci. Sinter. 16 (1984), 97–104.
[4] D. Simwonis, F. Tietz, D. Stover, Solid State Ionics 132 (2000), 241–251.
[5] J. S. Cronin, J. R. Wilson, S. A. Barnett, Journal of Power Sources 196 (2011), 2640-2643.
[6] R. Davis, F. Abdeljawad, J. Lillibridge, M. Haataja, Acta Materialia 78 (2014), 271-281.
[7] A. Faes, A. Hessler-Wyser, D. Presvytes, C.G. Vayenas, J. Van Herle, Fuel Cells 9 (2009), 841–851.
[8] P. Tanasini, M. Cannarozzo, P. Costamagna, A. Faes, J. Van Herle, A. Hessler-Wyser, C. Comninellis, Fuel Cells 9 (2009), 740–75.
[9] H. Chen, H Yu, J. S. Cronin, J. R. Wilson, S. A. Barnett, K. Thornton, Journal of Power Sources 196 (2011), 1333-1337.
[10] D. Kennouche, Y. K. Chen-Wiegart, K. J. Yakal-Kremski, J. Wang, J. W. Gibbs, P. W. Voorhees, S. A. Barnett, Acta Materialia 103 (2016), 204-210.
[11] F. Abdeljawad, B. Völker, R. Davis, R. M. McMeeking, M. Haataja, Journal of Power Sources 250 (2014), 319-331.
[12] A. Nakajo, A. P. Cocco, M. B. Degostin, P. Burdet, A. A. Peracchio, B. N. Cassenti, M. Cantoni, J. Van herle, W. K. S. Chiu, ECS Transactions 78 (1) (2017), 3205-3215.
[13] G. Rinaldi, S. Diethelm, E. Oveisi, P. Burdet, J. Van herle, D. Montinaro, Q. Fu, A. Brisse, Fuel Cells 17 (4) (2017), 541-549.
[14] K. N. Grew, Y. S. Chu, J. Yi, A. A. Peracchio, J. R. Izzo, Y. Hwu, F. De Carlo, W. K. S. Chiu, Journal of The Electrochemical Society 157 (6) (2010), B783-B792.
[15] D. Chen, Z. Lin, H. Zhu, R. J. Kee, Journal of Power Sources 191 (2) (2009), 240–252.

Remark: Only the abstract is officially available, because the authors publish elsewhere. Please see Presentations on www.EFCF.com/LIB or contact the authors directly.